

Steady-State Rate-Optimal Power Adaptation in Energy Harvesting Opportunistic Cognitive Radios with Spectrum Sensing and Channel Estimation Errors

Hassan Yazdani, Azadeh Vosoughi, *Senior Member, IEEE*

Abstract—We consider an opportunistic cognitive radio network, consisting of N_u secondary users (SUs) and an access point (AP), that can access a spectrum band licensed to a primary user. Each SU is capable of harvesting energy, and is equipped with a finite size battery, for energy storage. The SUs operate under a time-slotted scheme, where each time slot consists of three non-overlapping phases: spectrum sensing phase, channel probing phase, and data transmission phase. The AP feeds back its estimates of fading coefficients of SUs–AP link to SUs. To strike a balance between the energy harvesting and the energy consumption, we propose a parametrized power control strategy that allows each SU to adapt its power, according to the feedback information and its stored energy. Modeling the randomly arriving energy packets during a time slot as a Poisson process, we establish a lower bound on the achievable sum-rate of SUs–AP links, in the presence of both spectrum sensing and channel estimation errors. We optimize the parameters of the proposed power control strategy, such that the derived sum-rate lower bound is maximized, subject to an interference constraint. Via simulations, we corroborate our analysis and explore spectrum sensing-channel probing-data transmission trade-offs.

Index Terms—opportunistic cognitive radio, energy harvesting, imperfect spectrum sensing, channel estimation, constrained sum-rate maximization, average interference power constraint, finite-size battery, steady-state battery operation, adaptive transmission power.

I. INTRODUCTION

A. Literature Review

The explosive rise in demand for high data rate wireless applications has turned the spectrum into a scarce resource. Cognitive radio (CR) technology is a promising solution which alleviates spectrum scarcity problem by allowing an unlicensed secondary user (SU) to access licensed frequency bands in a such way that its imposed interference on primary users (PUs) is limited [1]–[3]. Therefore, CR systems can increase spectrum efficiency significantly. CR systems are mainly classified as underlay CR and opportunistic CR systems. In underlay CR systems, SUs use a licensed frequency band simultaneously with PUs, conditioned that the interference power imposed on PUs (caused by SUs) remains below a pre-determined level. In opportunistic CR systems, SUs use a licensed frequency band as long as the frequency band is not used by PUs. While opportunistic CR systems do not require coordination between PUs and SUs to acquire channel state information

(CSI) corresponding to SU-PU link, they necessitate spectrum sensing to monitor and detect PUs' activities and protect PUs against harmful interference caused by SUs [4]–[6]. In these systems, the status of PUs' activities (being busy or idle) and the duration of spectrum sensing affect the system performance [5]–[9]. Spectrum sensing is prone to errors (characterized in terms of mis-detection and false alarm probabilities) which need to be considered in the system design. Another important factor that impacts the performance of opportunistic CR systems is the level of assumption made regarding the availability of CSI. In opportunistic CR systems, although CSI corresponding to SU-PU link is not required (which is a major advantage), still CSI corresponding to SU transmitter–SU receiver (SU_{tx}–SU_{rx}) link is needed for properly adapting the data transmission.

In addition to spectral efficiency, energy efficiency is another important metric to consider when designing communication systems [10]–[16]. Energy harvesting (EH) has been recognized as an effective approach for improving the energy efficiency. EH-powered devices can operate without the need for external power cables or periodic battery replacements [17], [18]. EH-enabled CR systems have received substantial attention as a promising solution for increasing both energy efficiency and spectral efficiency [19]–[21]. EH-enabled communication systems can harvest energy from ambient energy sources (e.g., solar, wind, thermal, vibration) or radio frequency (RF) signals. For instance, in an ambient RF EH-enabled CR system, the energy of emitted RF signals from TV/radio broadcast towers, cellular base stations, and Wi-Fi access points (APs) is captured by SU_{tx} antenna and stored in its battery [22]–[26]. A dedicated RF signal source can be utilized for energy harvesting and enabling simultaneous wireless information and power transfer (SWIPT) [27], [28].

The body of research on EH-enabled communication systems can be grouped into two main categories, depending on the adopted energy arrival model [10], [29]: in the first model, the energy arrival is deterministic and the transmitter has a causal or non-causal knowledge of the energy arrival at the beginning of transmission [30]. In the second model, the energy arrival is stochastic [10]. In practice, the energy arrival of ambient energy sources, including ambient RF signal sources, is intrinsically time-variant and often sporadic. This natural factor degrades the performance of the battery-free EH-enabled communication systems in which a “harvest-then-

transmit” strategy is adopted, i.e., users can only transmit when the energy harvested in one time slot is sufficient for data transmission [31]. To flatten the randomness of the energy arrival, the harvested energy is stored in a battery, to balance the energy arrival and the energy consumption [10]. In practice, the capacity of the batteries is limited, and this can result in an energy overflow.

Power/energy management in EH-enabled communication systems with finite size batteries is necessary, in order to adapt the rate of energy consumption with the rate of energy harvesting. If the energy management policy is overly aggressive, such that the rate of energy consumption is greater than the rate of energy harvesting, the transmitter may stop functioning, due to energy outage. On the other hand, if the energy management policy is overly conservative, the transmitter may fail to utilize the excess energy, due to energy overflow, and the data transmission would become limited in each energy allocation interval.

Focusing on opportunistic EH-enabled CR systems, we realize that power control strategies, aiming at optimizing the performance of SUs, should be designed such that spectrum sensing (and its corresponding errors), as well as spectrum sensing-data transmission trade-offs are incorporated in the design process. For instance, the authors in [22] considered a system model, where SU_{tx} can perform energy harvesting and spectrum sensing simultaneously. Depending on the results of spectrum sensing, SU_{tx} continues to harvest energy (when the spectrum is sensed busy) or transmits data (when the spectrum is sensed idle), and studied maximizing SU_{tx} - SU_{rx} channel capacity, via optimizing the threshold of the energy detector (employed for spectrum sensing). Aiming at a similar goal (i.e., maximizing the SU’s channel capacity), the authors in [26] considered a modified system model, where SU_{tx} cannot perform energy harvesting and spectrum sensing at the same time. The authors investigated the optimal mode selection policy (i.e., to choose whether to access the spectrum or to harvest energy) for CR sensor networks. Targeting the same goal as [22], [26], the authors in [7], [16] studied the optimal allocation of energy to be consumed for spectrum sensing versus data transmission, assuming that SU_{tx} has a finite size data buffer. The authors in [8] considered a different system model, where energy harvesting, spectrum sensing, and data transmission occur in three non-overlapping time intervals within a frame. They studied maximizing the SU_{tx} - SU_{rx} link throughput, via optimizing the duration of spectrum sensing and the threshold of the energy detector (for spectrum sensing), and investigated the energy harvesting-spectrum sensing-data transmission trade-offs. We note that the works in [7], [8], [16], [22], [26] assume that CSI of SU_{tx} - SU_{rx} link is perfectly known at both SU_{tx} and SU_{rx} .

In general, the power control strategies designed for opportunistic EH-enabled CR systems should depend on the level of assumption made regarding the availability of CSI corresponding to SU_{tx} - SU_{rx} link, and whether the adapted transmit power levels are continuous or discrete values. In practice, only partial CSI can be available at SU_{tx} and SU_{rx} due to several factors (e.g., channel estimation error and limitation of feedback channel from SU_{rx} to SU_{tx}). Partial CSI has

deteriorating effects on the performance of communication systems (including EH-enabled CR systems), and should not be overlooked. In the following, we reference several works that consider the effects of partial CSI on the performance of EH-enabled communication systems, with stochastic energy arrival model and finite size batteries. Assuming perfect CSI at the receiver (Rx) and quantized CSI (due to limited feedback channel) at the transmitter (Tx), the authors in [32] aimed at maximizing the Tx’s bit rate, via adapting discrete-valued data transmit power and modulation order, according to the quantized CSI of Tx-Rx link and the Tx battery state. Assuming perfect CSI at the Rx and single-bit partial CSI at the Tx (due to severely limited feedback channel), the authors in [30] targeted at maximizing the Tx-Rx link throughput, via optimizing the threshold of the binary channel quantizer and discrete-valued data transmit power. Assuming perfect CSI at the Rx and partial CSI at the Tx (due to channel estimation error), the authors in [29], [33] analyzed maximizing the Tx’s average throughput, in two asymptotic regimes (where the rate of energy harvesting is very small or very large), via optimizing continuous-valued data transmit power. We note that, none of the referenced works in [29], [30], [32], [33] considered CR systems. Furthermore, these works assume that CSI is perfectly known at the Rx.

B. Knowledge Gap and Our Contributions

We consider an opportunistic EH-enabled CR network, consisting of N_u SUs and an access point (AP), that can access a wideband spectrum licensed to a primary network. Each SU is capable of harvesting energy from natural ambient energy sources, and is equipped with a finite size rechargeable battery, to store the harvested energy. Our main *objectives* are (i) to study how the achievable sum-rate of SUs is impacted by the *combined effects* of spectrum sensing error and imperfect CSI of SUs-AP links (due to channel estimation error), and (ii) to design an energy management strategy that maximizes the achievable sum-rate of SUs, subject to a constraint on the average interference power that SUs can impose on the PU. To the best of our knowledge, our work is the first to study the impact of these combined effects on the performance of an opportunistic EH-enabled CR network.

The importance of our study is evident by the works in [34]–[39], which demonstrate the significance of considering the effect of imperfect CSI at the Rx, due to channel estimation, on the Tx achievable rate. We note that the Tx in these works is a primary transmitter (not a secondary transmitter in a CR system) and has a traditional stable power supply. One expects that spectrum sensing error, combined with random energy arrival at the Tx, exacerbates the effect of imperfect CSI on the Tx achievable rate. The challenges of our study are twofold: first, it requires integration of energy harvesting, spectrum sensing, and channel estimation. Successful achievement of this integration entails stochastic modeling of energy arrival, energy storage, and PU’s activities. These stochastic models are utilized to establish an achievable sum-rate of SUs that takes into account both spectrum sensing error and channel estimation error. Second, one needs to properly design energy

control strategies for SUs, that strike a balance between the energy harvesting and the energy consumption, and adapt transmit power according to the available CSI and the battery state.

We assume that SUs operate under a time-slotted scheme, and SU_n is capable of harvesting energy during the entire time slot. Each time slot consists of three sub-slots corresponding to spectrum sensing phase (during which SU_n senses the spectrum), channel probing phase (during which SU_n sends pilot symbols to the AP, when the spectrum is sensed idle, for estimating the fading coefficient corresponding to SU_n -AP link), and data transmission phase (during which SU_n sends data symbols to the AP). Assuming that the AP feeds back its estimate of the fading coefficient to SU_n , SU_n adapts its transmit power based on this information as well as the available energy in its battery.

Our main contributions can be summarized as follow:

- 1) Our system model encompasses the stochastic energy arrival model for harvesting energy, the stochastic energy storage model for the finite size battery, the stochastic model of PU's activities, spectrum sensing error, and channel estimation error (both at SUs and the AP). We model the randomly arriving energy packets during a time slot as a Poisson process, and the dynamics of the battery as a finite state Markov chain.
- 2) We propose a power adaptation strategy for SU_n that mimics the behavior of the rate-optimal power adaptation scheme with respect to the estimated channel power gain \hat{g}_n available at SU_n and the AP, i.e., when \hat{g}_n is below a cut-off threshold θ_n , the transmit energy is zero, and when \hat{g}_n exceeds θ_n , the transmit energy increases monotonically in proportion to a parameter Ω_n , as \hat{g}_n increases. The parameters Ω_n and θ_n play key roles in balancing the energy harvesting and the energy consumption.
- 3) Given our system model, we establish a lower bound on the achievable sum-rate of SUs-AP links, in the presence of both spectrum sensing error and channel estimation error (both at SUs and the AP). We formulate a novel constrained optimization problem with the optimization variables $\{\Omega_n, \theta_n\}_{n=1}^{N_u}$, aiming at maximizing the derived sum-rate lower bound, subject to the average interference constraint (AIC) imposed on the PU and the causality constraint of the battery. We solve the formulated constrained optimization problem assuming that the battery reaches its steady-state.
- 4) We derive closed form expressions for the battery outage probability and transmission outage probability and demonstrate their behaviors, in terms of the average number of harvesting energy packets and the AIC. We also study the existing trade-offs between spectrum sensing-channel probing-data transmission and how these trade-offs impact the sum-rate of our CR network.

Our work is different from [29]–[32]. In particular, these works view the energy management policy design as a sequential decision making problem, and hence, they adopt the Markov decision process (MDP) framework to solve the problem. In this framework, the goal is typically optimizing a specific metric over a horizon spanning several time slots. The solutions (obtained using dynamic programming) are dependent across time slots, and also depend on the initial condition

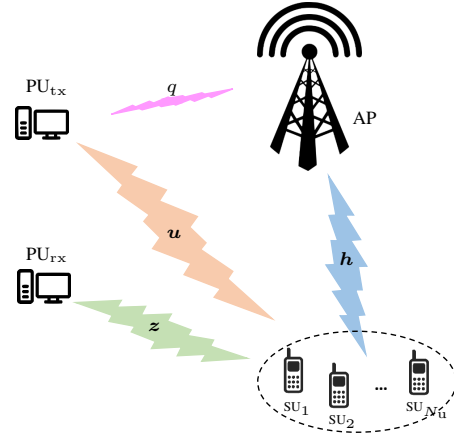


Fig. 1: Schematics of the uplink CR network.

(i.e., the initial state of the battery). Here, we assume that the battery operates at its steady-state, and hence, our proposed constrained optimization problem can be solved for each time slot. Furthermore, the problem can be solved *offline* and the optimized transmission parameters $\{\Omega_n, \theta_n\}_{n=1}^{N_u}$ (that do *not* depend on the initial condition of the battery) can become available *a priori* at the AP and SUs. During the data transmission phase, SU_n chooses its symbol power, using its optimized transmission parameters Ω_n, θ_n , and based on its partial CSI of SU_n -AP link (received via the feedback channel) as well as the available energy in its battery.

C. Paper Organization

The remainder of the paper is organized as follows. Section II explains our system model. Section III describes the spectrum sensing phase and our binary energy-based detector for detecting PU activity. Section IV discusses the channel probing phase. Section V explains the data transmission phase and derives a lower bound on the achievable sum-rate of our CR network. Also, it formulates our proposed constrained optimization problem. Section VI corroborates our analysis on the proposed optimization problem with Matlab simulations. Section VII concludes the paper.

II. SYSTEM MODEL

We consider an uplink opportunistic CR network that can access a wideband spectrum band licensed to a primary network, consisting of M non-overlapping narrowband spectrum bands, each with a bandwidth of W Hz [3]. The primary network consists of a primary transmitter (PU_{tx}) and a primary receiver (PU_{rx}). The secondary network consists of an AP and N_u SUs (see Fig. 1). The AP can serve up to M SUs simultaneously and we assume that $N_u \leq M$. We also assume that narrowband spectrum bands are pre-assigned to SUs and thus each SU knows which band to sense and transmit data over. The SUs are equipped with identical energy harvesting circuits to harvest energy from the ambient environment and identical finite size batteries for energy storage (see Fig. 2). We consider block fading channel model and suppose flat fading

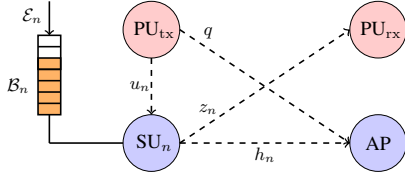


Fig. 2: Our CR system model corresponding to SU_n for $n = 1, \dots, N_u$.

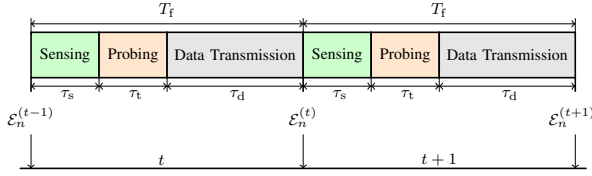


Fig. 3: Slot structure of SUs.

coefficients from PU_{tx} to SU_n , PU_{tx} to AP , SU_n to PU_{rx} , and SU_n to AP are four independent zero-mean complex Gaussian random variables, which we denote by u_n , q , z_n and h_n with variances δ_{u_n} , δ_q , δ_{z_n} and γ_n , respectively.

A. Battery and Energy Harvesting Models

We assume that SUs operate under a time-slotted scheme, with slot duration of T_f seconds, and they always have data to transmit. Each time slot is indexed by an integer t for $t = 1, 2, \dots$. The energy harvester at each SU stores randomly arrived energy in a finite size battery and consumes the stored energy for spectrum sensing, channel probing, and data transmission. Each battery consists of K cells (units) and the amount of energy stored in each unit is equal to e_u Joules. Thus, the battery can store up to Ke_u Joules of energy.

When k cells of the battery is charged (the amount of stored energy in the battery is ke_u Joules) we say that the battery is at state k . Let $\mathcal{B}_n^{(t)} \in \{0, 1, \dots, K\}$ denote the discrete random process indicating the battery state of SU_n at the beginning of time slot t . We define the probability mass function (pmf) of the discrete random variable $\mathcal{B}_n^{(t)}$ as $\zeta_{k,n}^{(t)} = \Pr(\mathcal{B}_n^{(t)} = k)$, where $\sum_{k=0}^K \zeta_{k,n}^{(t)} = 1$. Note that $\mathcal{B}_n^{(t)} = 0$ and $\mathcal{B}_n^{(t)} = K$ represent the empty battery and full battery levels, respectively.

Let $\mathcal{E}_n^{(t)}$ denote the randomly arriving energy packets during time slot t of SU_n , where the energy packet measured in Jules is e_u Jules. The discrete random process $\mathcal{E}_n^{(t)}$ is typically modeled as a sequence of independent and identically distributed (i.i.d.) random variables [16], regardless of the spectrum occupancy state of PU_{tx} . We assume that the discrete random variables $\mathcal{E}_n^{(t)}$'s are i.i.d. over time and independent across sensors. We model $\mathcal{E}_n^{(t)}$ as a Poisson random variable with the pmf $f_{\mathcal{E}_n}(r) = \Pr(\mathcal{E} = r) = e^{-\rho_n} \rho_n^r / r!$ for $r = 0, 1, \dots, \infty$, where ρ_n denotes the average number of arriving energy packets during one time slot of SU_n .¹ Let $\alpha_{h_n}^{(t)}$ be the number of stored (harvested) energy units in the

¹We note that ρ_n does not depend on the duration of spectrum sensing phase, since we assume each node is capable of harvesting energy during the entire slot. If we limit harvesting energy to spectrum sensing phase, then ρ_n would change to $\rho_n \tau_s / T_f$.

battery at SU_n during time slot t . This harvested energy cannot be used during time slot t . Since the battery has a finite capacity of K cells, $\alpha_{h_n}^{(t)} \in \{0, 1, \dots, K\}$. Also, $\alpha_{h_n}^{(t)}$ are i.i.d. over time slots and independent across sensors. Let $f_{\alpha_{h_n}}(r) = \Pr(\alpha_{h_n} = r)$ denote the pmf of $\alpha_{h_n}^{(t)}$. We can find the pmf of $\alpha_{h_n}^{(t)}$ in terms of the pmf of $\mathcal{E}_n^{(t)}$ as the following

$$f_{\alpha_{h_n}}(r) = \begin{cases} f_{\mathcal{E}_n}(r), & \text{if } 0 \leq r \leq K-1 \\ \sum_{m=K}^{\infty} f_{\mathcal{E}_n}(m), & \text{if } r = K. \end{cases} \quad (1)$$

B. Slot Structure of SUs

Each time slot consists of three sub-slots (see Fig. 3), corresponding to spectrum sensing phase, channel probing phase, and data transmission phase, with fixed durations of $\tau_s = N_s / f_s$, $\tau_t = N_t / f_s$, $\tau_d = N_d / f_s$, respectively. Note that f_s is the sampling frequency, N_s is the number of collected samples during spectrum sensing phase, N_t is the number of training symbols sent during channel probing phase, and N_d is the number of data symbols sent during data transmission phase. Also, we have $T_f = \tau_s + \tau_t + \tau_d$.

During *spectrum sensing phase*, SU_n senses its pre-assigned single spectrum band to detect PU_{tx} 's activity. We model the PU_{tx} 's activity in each spectrum band as a Bernoulli random variable and we assume the statistics of PU_{tx} are i.i.d. across M spectrum bands and over time slots. Therefore, we can frame the spectrum sensing problem at SU_n as a binary hypothesis testing problem. Suppose $\mathcal{H}_1^{(t)}$ and $\mathcal{H}_0^{(t)}$ represent the binary hypotheses of PU_{tx} being active and inactive in time slot t , respectively, with prior probabilities $\Pr\{\mathcal{H}_1^{(t)}\} = \pi_1$ and $\Pr\{\mathcal{H}_0^{(t)}\} = \pi_0$. SU_n applies a binary detection rule to decide whether or not PU_{tx} is active in its pre-assigned band. Let $\hat{\mathcal{H}}_{0,n}$ and $\hat{\mathcal{H}}_{1,n}$, with probabilities $\hat{\pi}_{0,n} = \Pr\{\hat{\mathcal{H}}_{0,n}\}$ and $\hat{\pi}_{1,n} = \Pr\{\hat{\mathcal{H}}_{1,n}\}$ denote the SU_n detector outcome, i.e., the detector finds PU_{tx} active and inactive (the result of spectrum sensing is busy or idle), respectively. The accuracy of this binary detector is characterized by its false alarm and detection probabilities. The details of the binary detector are presented in Section III.

Depending on the outcome its of spectrum sensing, SU_n stays in spectrum sensing phase or enters *channel probing phase*. In this phase, SU_n sends N_t training symbols with fixed symbol power $P_t = \alpha_t e_u / \tau_t$, to enable channel estimation at the AP, where α_t is the number of consumed cells of energy for channel probing². We assume that the battery always has α_t units of stored energy for channel probing. Let $h_n^{(t)}$ denote the SU_n -AP fading coefficient in time slot t and $g_n^{(t)} = |h_n^{(t)}|^2$ be the corresponding channel power gain. Using the received signals corresponding to the training symbols, the AP estimates $\hat{h}_n^{(t)}$ and lets $\hat{g}_n^{(t)} = |\hat{h}_n^{(t)}|^2$ and shares this value with SU_n via a feedback channel. Next, SU_n enters *data transmission phase*. During this phase, SU_n sends N_d Gaussian data symbols with adaptive symbol power according to its battery state and the received information via

²For ease of presentation, we assume that circuit power (energy) consumption is negligible in comparison to the consumed energy for channel probing and data transmission. Otherwise, it can easily be incorporated into the system model.

the feedback channel about SU_n-AP link. If the battery is at state k , then SU_n allocates $\alpha_{k,n}$ cells of stored energy for each data symbol transmission, implying that the adaptive symbol power is $P_{k,n}^{(t)} = \alpha_{k,n}^{(t)} p_u$, where $p_u = e_u / \tau_d$. Note that since $\alpha_{k,n}^{(t)}$ is discrete, $P_{k,n}^{(t)}$ is discrete. The details of the choice of $\alpha_{k,n}^{(t)}$ according to the battery state k and the feedback information \hat{g}_n are given in Section II-C and the details of channel estimation are explained in Section IV.

C. Transmission Model and Battery Dynamics

As we said, we assume that SU_n adapts its transmit energy per data symbol (power) according to its battery state k and the received information via the feedback channel about its channel power gain \hat{g}_n . In particular, we choose a power adaptation strategy that mimics the behavior of the rate-optimal power adaptation scheme with respect to the channel power gain [6], i.e., when \hat{g}_n is smaller than a cut-off threshold θ_n (to be optimized), the transmit energy is zero, and when \hat{g}_n exceeds θ_n , the transmit energy increases monotonically as \hat{g}_n increases until it reaches its maximum value of $\lfloor k\Omega_n \rfloor - \alpha_t$, where $\Omega_n \in [0, 1]$ (to be optimized), and $\lfloor \cdot \rfloor$ denotes the floor function. Mathematically, we express $\alpha_{k,n}^{(t)}$ for SU_n as the following

$$\alpha_{k,n}^{(t)} = \max \{ \bar{\alpha}_{k,n}^{(t)}, 0 \}, \quad \text{for } k = 0, 1, \dots, K, \quad (2a)$$

$$\bar{\alpha}_{k,n}^{(t)} = \left\lfloor \Omega_n k \left(1 - \frac{\theta_n}{\hat{g}_n^{(t)}} \right)^+ \right\rfloor - \alpha_t, \quad (2b)$$

where $(x)^+ = \max\{x, 0\}$. The parameters Ω_n and θ_n in (2) play key roles in balancing the energy harvesting and the energy consumption. Given θ_n , when Ω_n is large (or given Ω_n , when θ_n is small), such that the rate of energy consumption is greater than the rate of energy harvesting, SU_n may stop functioning, due to energy outage. On the other hand, given θ_n , when Ω_n is small (or given Ω_n , when θ_n is large), SU_n may fail to utilize the excess energy, due to energy overflow, and the data transmission would become limited in each slot. Note that $\bar{\alpha}_{k,n}^{(t)}$ in (2) ensures that the battery always has α_t units of stored energy for channel probing. Furthermore, the transmission policy in (2) satisfies the causality constraint of the battery. The causality constraint restrains the energy corresponding to symbol transmit power to be less than the available stored energy in the battery, i.e., $\alpha_{k,n} \leq k - \alpha_t$. Note that $\alpha_{k,n}$ is discrete random variable and $\alpha_{k,n} \in \{0, 1, \dots, K\}$. Let $\psi_{i,k,n}^\varepsilon = \Pr(\alpha_{k,n} = i | \mathcal{H}_\varepsilon)$ denote the pmf of $\alpha_{k,n}$ given $\mathcal{H}_\varepsilon, \varepsilon = 0, 1$. We have

$$\psi_{i,k,n}^\varepsilon = \begin{cases} 1, & \text{if } 0 \leq k \leq \alpha_t, i = 0 \\ 0, & \text{if } 0 \leq k \leq \alpha_t, i \neq 0 \\ Y_{k,n}, & \text{if } k \geq \alpha_t + 1, i = 0 \\ Q_{i,k,n}, & \text{if } k \geq \alpha_t + 1, 1 \leq i \leq \lfloor k\Omega_n \rfloor - \alpha_t \\ 0, & \text{if } k \geq \alpha_t + 1, i \geq \lfloor k\Omega_n \rfloor - \alpha_t + 1 \end{cases} \quad (3)$$

in which

$$Q_{i,k,n} = F_{\hat{g}_n}^\varepsilon(c_{i,k,n}) - F_{\hat{g}_n}^\varepsilon(a_{i,k,n}) \quad (4a)$$

$$Y_{k,n} = F_{\hat{g}_n}^\varepsilon(\theta_n) + \sum_{m=1}^{\min(\lfloor k\Omega_n \rfloor, \alpha_t)} Q_{m-\alpha_t, k, n} \quad (4b)$$

$$a_{i,k,n} = \frac{\theta_n k \Omega_n}{k \Omega_n - \alpha_t - i}, \quad c_{i,k,n} = \frac{\theta_n k \Omega_n}{k \Omega_n - \alpha_t - i - 1}, \quad (4c)$$

where $F_{\hat{g}_n}^\varepsilon(x) = F_{\hat{g}_n}(x | \mathcal{H}_\varepsilon)$ is the cumulative distribution function (CDF) of \hat{g}_n given \mathcal{H}_ε . Note that if $c_{i,k,n} < 0$, we set $c_{i,k,n} = +\infty$.

The battery state at the beginning of time slot $t+1$ depends on the battery state at the beginning of time slot t , the harvested energy during time slot t , the transmission symbol, as well as α_t . In particular, if at time slot t , SU_n senses its spectrum band to be idle, the state of its battery at the beginning of slot $t+1$ is

$$\mathcal{B}_n^{(t+1)} = \min \left\{ \left(\mathcal{B}_n^{(t)} - \alpha_t - \alpha_{k,n}^{(t)} + \alpha_{h_n}^{(t)} \right)^+, K \right\}. \quad (5)$$

On the other hand if at time slot t , SU_n senses its spectrum band to be busy, the state of its battery at the beginning of slot $t+1$ is

$$\mathcal{B}_n^{(t+1)} = \min \left\{ \left(\mathcal{B}_n^{(t)} + \alpha_{h_n}^{(t)} \right)^+, K \right\}, \quad (6)$$

since $\alpha_{k,n}^{(t)} = 0$. Considering the dynamic battery state model in (5) and (6) we note that, conditioned on $\alpha_{h_n}^{(t)}$ and $\alpha_{k,n}^{(t)}$ the value of $\mathcal{B}_n^{(t+1)}$ only depends on the value of $\mathcal{B}_n^{(t)}$ (and not the battery states of time slots before t). Hence, the battery state random process $\mathcal{B}_n^{(t)}$ can be modeled as a Markov chain. Let the probability vector of battery state in time slot t be $\zeta_n^{(t)} = [\zeta_{1,n}^{(t)}, \dots, \zeta_{K,n}^{(t)}]^T$. Note that the probability $\zeta_{k,n}^{(t)}$ depends on the battery state at slot $t-1$, the number of battery units filled by the harvested energy during slot $t-1$, the probability of spectrum band sensed idle, and, the number of energy units allocated for data transmission at slot $t-1$ when the spectrum band is sensed idle, i.e., $\zeta_{k,n}^{(t)}$ depends on $\mathcal{B}_n^{(t-1)}, \alpha_{h_n}^{(t-1)}, \hat{\pi}_{0,n}, \alpha_{k,n}^{(t-1)}$, respectively. Assuming the Markov chain is time-homogeneous, we let Φ_n denote the $(K+1) \times (K+1)$ transition probability matrix of this chain with its (i, j) -th entry $\phi_{i,j}^n = \Pr(\mathcal{B}_n^{(t)} = i | \mathcal{B}_n^{(t-1)} = j)$ given in (7) where $F_{\alpha_{h_n}}(\cdot)$ is the commutative distribution function (CDF) of α_{h_n} . We have

$$\zeta_n^{(t+1)} = \Phi_n \zeta_n^{(t)}. \quad (8)$$

Since the Markov chain characterized by the transition probability matrix Φ_n is irreducible and aperiodic, there exists a unique steady-state distribution, regardless of the initial state [40]. Let $\zeta_n = \lim_{t \rightarrow \infty} \zeta_n^{(t)}$ be the unique steady-state probability vector. This vector satisfies the following equations

$$\zeta_n = \Phi_n \zeta_n, \quad (9a)$$

$$\zeta_n^T \mathbf{1} = \sum_{k=1}^K \zeta_{k,n} = 1, \quad (9b)$$

$$\phi_{0,j}^n = \sum_{l=0}^K \left[\psi_{l,j,n}^0 \hat{\pi}_{0,n} F_{\alpha_{h_n}}(\alpha_t + l - j) \right] + \hat{\pi}_{1,n} F_{\alpha_{h_n}}(-j) \quad (7a)$$

$$\phi_{K,j}^n = \sum_{l=0}^K \left[\psi_{l,j,n}^0 \hat{\pi}_{0,n} \left(1 - F_{\alpha_{h_n}}(\alpha_t + l + K - j) \right) \right] + \hat{\pi}_{1,n} \left(1 - F_{\alpha_{h_n}}(K - j) \right) \quad (7b)$$

$$\phi_{i,j}^n = \sum_{l=0}^K \left[\psi_{l,j,n}^0 \hat{\pi}_{0,n} f_{\alpha_{h_n}}(\alpha_t + l + i - j) \right] + \hat{\pi}_{1,n} f_{\alpha_{h_n}}(i - j), \quad \text{for } i = 1, \dots, K - 1 \quad (7c)$$

where $\mathbf{1}$ is an all-ones vector, i.e., ζ_n is the normalized eigenvector corresponding to the unit eigenvalue of Φ_n , such that the entries of ζ_n sums up to one. The closed-form expression for ζ_n is [41]

$$\zeta_n = (\Phi_n - I + B)^{-1} \mathbf{1}, \quad (10)$$

where B is an all-ones matrix and I is the identity matrix. From this point forward, we assume that the battery is at its steady-state and we drop the superscript t .

To illustrate our transmission model in (2) we consider the following simple numerical example. Assuming that the battery has $K = 7$ cells, Fig. 4 shows an example of $\alpha_{k,n}$ for our CR system for two sets of $\{\Omega_n, \theta_n\}$ given as $\Omega_n^{(a)} = 0.75, \theta_n^{(a)} = 0.02$ and $\Omega_n^{(b)} = 0.95, \theta_n^{(b)} = 0.05$. The corresponding transition probability matrices are given in the following

$$\Phi_n^{(a)} = \begin{pmatrix} 0.42 & 0.29 & 0.17 & 0.08 & 0.02 & 0 & 0 & 0 \\ 0.12 & 0.13 & 0.12 & 0.09 & 0.05 & 0.02 & 0 & 0 \\ 0.19 & 0.12 & 0.13 & 0.12 & 0.09 & 0.05 & 0.02 & 0 \\ 0.07 & 0.19 & 0.12 & 0.13 & 0.12 & 0.09 & 0.05 & 0.02 \\ 0.05 & 0.07 & 0.19 & 0.12 & 0.13 & 0.12 & 0.09 & 0.05 \\ 0.05 & 0.05 & 0.07 & 0.19 & 0.12 & 0.13 & 0.12 & 0.09 \\ 0.04 & 0.05 & 0.05 & 0.07 & 0.19 & 0.12 & 0.13 & 0.12 \\ 0.06 & 0.1 & 0.15 & 0.2 & 0.27 & 0.46 & 0.58 & 0.71 \end{pmatrix},$$

$$\Phi_n^{(b)} = \begin{pmatrix} 0.51 & 0.4 & 0.28 & 0.16 & 0.08 & 0.02 & 0 & 0 \\ 0.17 & 0.11 & 0.12 & 0.12 & 0.09 & 0.05 & 0.02 & 0 \\ 0.06 & 0.17 & 0.11 & 0.12 & 0.12 & 0.09 & 0.05 & 0.02 \\ 0.05 & 0.06 & 0.17 & 0.11 & 0.12 & 0.12 & 0.09 & 0.05 \\ 0.05 & 0.05 & 0.06 & 0.17 & 0.11 & 0.12 & 0.12 & 0.09 \\ 0.05 & 0.05 & 0.05 & 0.06 & 0.17 & 0.11 & 0.12 & 0.12 \\ 0.04 & 0.05 & 0.05 & 0.05 & 0.06 & 0.17 & 0.11 & 0.12 \\ 0.06 & 0.11 & 0.16 & 0.21 & 0.26 & 0.32 & 0.49 & 0.6 \end{pmatrix}.$$

Our goal is to find the transmission parameters $\{\Omega_n, \theta_n\}$ in (2b) for all SUs such that the sum-rate of our CR network is maximized, subject to a constraint on the average interference power that collective SUs can impose on PU_{rx} . We assume that this optimization problem is solved *offline* at AP, given the statistical information of fading channels, the number of samples collected during spectrum sensing phase N_s , the number of training symbols sent during channel probing phase N_t , and power of training symbols P_t . The solutions to this optimization problem, i.e., the optimal set $\{\Omega_n, \theta_n\}_{n=1}^{N_u}$ is available *a priori* at the AP and SUs, to be utilized for adapting

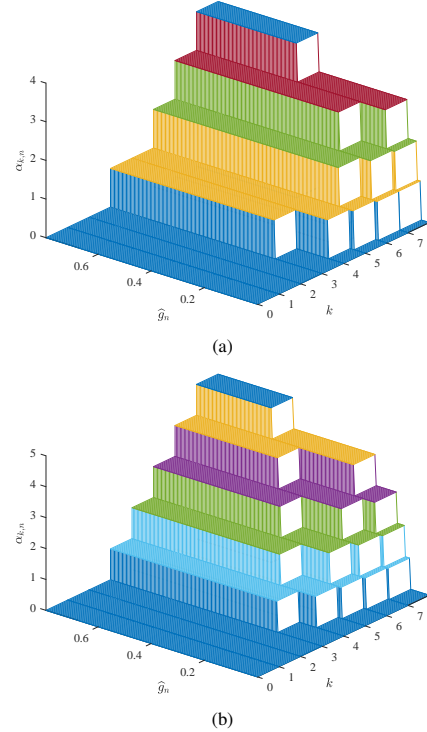


Fig. 4: This example shows how many energy units ($\alpha_{k,n}$) SU_n spends for data transmission, given its battery state and the received information about its channel gain via feedback link. (a) $\Omega_n^{(a)} = 0.75, \theta_n^{(a)} = 0.02$, (b) $\Omega_n^{(b)} = 0.95, \theta_n^{(b)} = 0.05$.

symbol power during data transmission phase. The idea of offline power allocation optimization with a limited feedback channel has been used before for distributed detection systems in wireless sensor networks [42]. In the following sections, we describe how SUs operate during spectrum sensing phase, channel probing phase, and data transmission phase. For the readers' convenience, we have collected the most commonly used symbols in Table I.

III. SPECTRUM SENSING PHASE

In order to access its spectrum band, SU_n first needs to sense its band during spectrum sensing phase, to determine whether it is busy or idle (see Fig. 3). We formulate the spectrum sensing at SU_n as a binary hypothesis testing problem, where the received signal at SU_n can be written as:

$$\begin{aligned} \mathcal{H}_0 &: y_n[m] = w_n[m], \\ \mathcal{H}_1 &: y_n[m] = u_n[m] p[m] + w_n[m], \end{aligned} \quad (12)$$

TABLE I: Most commonly used symbols.

Symbol	Description
N_s	Number of collected samples during <i>spectrum sensing phase</i>
N_t	Number of training symbols during <i>channel probing phase</i>
N_d	Number of data symbols during <i>data transmission phase</i>
P_t	Power of training symbols
$h_n, \hat{h}_n, \tilde{h}_n$	Fading coefficient of SU_n -AP link, LMMSE channel estimate, and its corresponding estimation error
$\gamma_n, \hat{\gamma}_n, \tilde{\gamma}_n$	Variances of $h_n, \hat{h}_n, \tilde{h}_n$
π_0, π_1	Prior probabilities of \mathcal{H}_0 and \mathcal{H}_1
$\hat{\pi}_{0,n}, \hat{\pi}_{1,n}$	Probabilities of spectrum bands being sensed idle or busy
$\zeta_{k,n}$	Probability of SU_n battery being at state k
u_n	Fading coefficient of PU_{tx} - SU_n link with variance δ_{u_n}
q	Fading coefficient of PU_{tx} -AP link with variance δ_q
z_n	Fading coefficient of SU_n - PU_{rx} link with variance δ_{z_n}

for $m = 1, \dots, N_s$, where $p[m]$ is the transmit signal of PU_{tx} , $w_n[m] \sim \mathcal{CN}(0, \sigma_{w_n}^2)$ is the additive white Gaussian noise (AWGN) at SU_n and $u_n[m]$ is the fading coefficient corresponding to PU_{tx} - SU_n channel. The two hypotheses \mathcal{H}_0 and \mathcal{H}_1 with probabilities π_0 and $\pi_1 = 1 - \pi_0$ denote the spectrum is truly idle and truly busy, respectively. We assume that π_0 and π_1 are known to SUs based on long-term spectrum measurements. For spectrum sensing we consider energy detector, where the decision statistics at SU_n is $Z_n = \frac{1}{N_s} \sum_{m=1}^{N_s} |y_n[m]|^2$. The accuracy of this detector is characterized by its false alarm probability $P_{fa_n} = \Pr(\hat{\mathcal{H}}_{1,n} | \mathcal{H}_0) = \Pr(Z_n > \xi_n | \mathcal{H}_0)$ and detection probability $P_{d_n} = \Pr(\hat{\mathcal{H}}_{1,n} | \mathcal{H}_1) = \Pr(Z_n > \xi_n | \mathcal{H}_1)$, where ξ_n is the local decision threshold. For large N_s , we can invoke central limit theorem and approximate the cumulative distribution function (CDF) of Z_n as Gaussian. Hence, P_{fa_n} and P_{d_n} can be expressed in terms of Q function as below [43]

$$P_{fa_n} = Q\left(\left(\frac{\xi_n}{\sigma_{w_n}^2} - 1\right)\sqrt{N_s}\right), \quad (13a)$$

$$P_{d_n} = Q\left(\left(\frac{\xi_n}{\sigma_{w_n}^2} - \nu_n - 1\right)\sqrt{\frac{N_s}{2\nu_n + 1}}\right), \quad (13b)$$

where $\nu_n = P_p \delta_{u_n} / \sigma_{w_n}^2$ and P_p is the average transmit power of PU_{tx} . For a given value of $P_{d_n} = \bar{P}_d$, the false alarm probability can be written as

$$P_{fa_n} = Q\left(\sqrt{2\nu_n + 1}Q^{-1}(\bar{P}_d) + \nu_n\sqrt{\tau_s f_s}\right). \quad (14)$$

The probabilities $\hat{\pi}_{0,n}$ and $\hat{\pi}_{1,n}$, are related to P_{d_n} and P_{fa_n} . In particular, we have $\hat{\pi}_{0,n} = \beta_{0,n} + \beta_{1,n}$ and $\hat{\pi}_{1,n} = 1 - \hat{\pi}_{0,n}$ where

$$\beta_{0,n} = \Pr\{\mathcal{H}_0, \hat{\mathcal{H}}_{0,n}\} = \pi_0(1 - P_{fa_n}), \quad (15a)$$

$$\beta_{1,n} = \Pr\{\mathcal{H}_1, \hat{\mathcal{H}}_{0,n}\} = \pi_1(1 - P_{d_n}). \quad (15b)$$

IV. CHANNEL PROBING PHASE

Depending on the outcome of its spectrum sensing, SU_n either stays in spectrum sensing phase (i.e., remains silent in the remaining of time slot) if its band is sensed busy (the detector outcome is $\hat{\mathcal{H}}_{1,n}$), or it enters channel probing phase if its band is sensed idle (the detector outcome is $\hat{\mathcal{H}}_{0,n}$). During channel probing phase, we assume SU_n sends training vector $\mathbf{x}_t = \sqrt{P_t} \mathbf{1}$, where $\mathbf{1}$ is an $N_t \times 1$ all-ones vector to enable channel estimation at the AP. Let vector $\mathbf{s}_n = [s_n(1), \dots, s_n(N_t)]^T$ denote the discrete-time

representation of received training symbols at the AP from SU_n . Assuming the fading coefficient h_n corresponding to SU_n -AP channel is unchanged during the entire time slot, we have

$$\begin{aligned} \mathcal{H}_0, \hat{\mathcal{H}}_{0,n}: \quad s_n[m] &= h_n \sqrt{P_t} + v_n[m], \\ \mathcal{H}_1, \hat{\mathcal{H}}_{0,n}: \quad s_n[m] &= h_n \sqrt{P_t} + q[m]p[m] + v_n[m], \end{aligned} \quad (16)$$

for $m = 1, \dots, N_t$, $v_n[m] \sim \mathcal{CN}(0, \sigma_{v_n}^2)$ is the AWGN at the AP, and $q[m]$ is the fading coefficient corresponding to PU_{tx} -AP channel. The linear minimum mean square error (LMMSE) estimate of h_n given $\hat{\mathcal{H}}_{0,n}$ is [6], [44]

$$\hat{h}_n = C_{h_n \mathbf{s}_n} C_{\mathbf{s}_n}^{-1} \mathbf{s}_n, \quad (17a)$$

$$C_{h_n \mathbf{s}_n} = \mathbb{E}\{h_n \mathbf{s}_n^H | \hat{\mathcal{H}}_{0,n}\} = \gamma_n \sqrt{P_t} \mathbf{1}, \quad (17b)$$

$$C_{\mathbf{s}_n} = \mathbb{E}\{\mathbf{s}_n \mathbf{s}_n^H | \hat{\mathcal{H}}_{0,n}\} = \omega_{0,n} \mathbb{E}\{\mathbf{s}_n \mathbf{s}_n^H | \mathcal{H}_0, \hat{\mathcal{H}}_{0,n}\} + \omega_{1,n} \mathbb{E}\{\mathbf{s}_n \mathbf{s}_n^H | \mathcal{H}_1, \hat{\mathcal{H}}_{0,n}\}, \quad (17c)$$

where

$$\omega_{0,n} = \Pr\{\mathcal{H}_0 | \hat{\mathcal{H}}_{0,n}\} = \frac{\pi_0(1 - P_{fa_n})}{\hat{\pi}_{0,n}} = \frac{\beta_{0,n}}{\hat{\pi}_{0,n}}, \quad (18a)$$

$$\omega_{1,n} = \Pr\{\mathcal{H}_1 | \hat{\mathcal{H}}_{0,n}\} = \frac{\pi_1(1 - P_{d_n})}{\hat{\pi}_{0,n}} = \frac{\beta_{1,n}}{\hat{\pi}_{0,n}}, \quad (18b)$$

and

$$\mathbb{E}\{\mathbf{s}_n \mathbf{s}_n^H | \mathcal{H}_0, \hat{\mathcal{H}}_{0,n}\} = (\hat{\gamma}_n^0 P_t + \sigma_{v_n}^2) \mathbf{I}, \quad (19a)$$

$$\mathbb{E}\{\mathbf{s}_n \mathbf{s}_n^H | \mathcal{H}_1, \hat{\mathcal{H}}_{0,n}\} = (\hat{\gamma}_n^1 P_t + \sigma_{v_n}^2 + \sigma_p^2) \mathbf{I}. \quad (19b)$$

After substituting (18) into (17), \hat{h}_n reduces to

$$\hat{h}_n = \frac{\gamma_n \sqrt{P_t}}{\gamma_n P_t N_t + \sigma_{v_n}^2 + \omega_{1,n} \sigma_p^2} \sum_{m=1}^{N_t} s_n[m], \quad (20)$$

where $\sigma_p^2 = P_p \delta_q$. The estimation error is $\tilde{h}_n = h_n - \hat{h}_n$, where \tilde{h}_n and \hat{h}_n are orthogonal random variables [44], and \tilde{h}_n and \hat{h}_n are zero mean. Approximating $q[m]p[m]$ as a zero-mean Gaussian random variable with variance σ_p^2 , we find that the estimate \hat{h}_n given $\hat{\mathcal{H}}_{0,n}$ is distributed as a Gaussian mixture random variable [6]. Let $\hat{\gamma}_n$ and $\tilde{\gamma}_n$, represent the variances of \hat{h}_n and \tilde{h}_n , respectively. Also, Let $\hat{\gamma}_n^0$ and $\hat{\gamma}_n^1$ represent the variances of \hat{h}_n under $\{\mathcal{H}_0, \hat{\mathcal{H}}_{0,n}\}$ and $\{\mathcal{H}_1, \hat{\mathcal{H}}_{0,n}\}$, respectively. We have

$$\hat{\gamma}_n^0 = \mathbb{V}\text{AR}\{\hat{h}_n | \mathcal{H}_0, \hat{\mathcal{H}}_{0,n}\} = \frac{\gamma_n^2 P_t N_t (\gamma_n P_t N_t + \sigma_{v_n}^2)}{(\gamma_n P_t N_t + \sigma_{v_n}^2 + \omega_{1,n} \sigma_p^2)^2}, \quad (21a)$$

$$\hat{\gamma}_n^1 = \mathbb{V}\text{AR}\{\hat{h}_n | \mathcal{H}_1, \hat{\mathcal{H}}_{0,n}\} = \frac{\gamma_n^2 P_t N_t (\gamma_n P_t N_t + \sigma_{v_n}^2 + \sigma_p^2)}{(\gamma_n P_t N_t + \sigma_{v_n}^2 + \omega_{1,n} \sigma_p^2)^2}. \quad (21b)$$

Therefore, $\hat{\gamma}_n = \omega_{0,n} \hat{\gamma}_n^0 + \omega_{1,n} \hat{\gamma}_n^1$. Also, let $\tilde{\gamma}_n^0$ and $\tilde{\gamma}_n^1$ indicate the variances of \tilde{h}_n under $\{\mathcal{H}_0, \hat{\mathcal{H}}_{0,n}\}$ and $\{\mathcal{H}_1, \hat{\mathcal{H}}_{0,n}\}$, respectively. We have

$$\tilde{\gamma}_n^0 = \mathbb{V}\text{AR}\{\tilde{h}_n | \mathcal{H}_0, \hat{\mathcal{H}}_{0,n}\} = \gamma_n - \hat{\gamma}_n^0, \quad (22a)$$

$$\tilde{\gamma}_n^1 = \mathbb{V}\text{AR}\{\tilde{h}_n | \mathcal{H}_1, \hat{\mathcal{H}}_{0,n}\} = \gamma_n - \hat{\gamma}_n^1. \quad (22b)$$

Hence, $\tilde{\gamma}_n = \omega_{0,n} \tilde{\gamma}_n^0 + \omega_{1,n} \tilde{\gamma}_n^1$. For ideal spectrum sensing, we get $\omega_{0,n} = 1$ and $\omega_{1,n} = 0$ and \hat{h}_n becomes Gaussian. Let $F_{g_n}^\varepsilon(x)$ denote the CDF of \hat{g}_n under $\{\mathcal{H}_\varepsilon, \hat{\mathcal{H}}_{0,n}\}$ for $\varepsilon = 0, 1$.

Note that under $\{\mathcal{H}_\varepsilon, \hat{\mathcal{H}}_{0,n}\}$ for $\varepsilon = 0, 1$, \hat{h}_n is zero mean complex Gaussian. Hence, under $\{\mathcal{H}_\varepsilon, \hat{\mathcal{H}}_{0,n}\}$ for $\varepsilon = 0, 1$, \hat{g}_n is an exponential random variable with mean $\tilde{\gamma}_n^\varepsilon$ and CDF

$$F_{\hat{g}_n}^\varepsilon(x) = 1 - e^{-\frac{x}{\tilde{\gamma}_n^\varepsilon}}. \quad (23)$$

The CDF of \hat{g}_n , denoted as $F_{\hat{g}_n}^\varepsilon(x)$, can be expressed in terms of $F_{\hat{g}_n}^0(x)$ and $F_{\hat{g}_n}^1(x)$ as the following:

$$F_{\hat{g}_n}(x) = \omega_{0,n} F_{\hat{g}_n}^0(x) + \omega_{1,n} F_{\hat{g}_n}^1(x). \quad (24)$$

After channel estimation, the AP feeds back the channel gains $\hat{g}_n = |\hat{h}_n|^2$ over a feedback link to SU_n .

V. DATA TRANSMISSION PHASE

After channel probing phase, SU_n enters this phase. We note that entering this phase is only possible, if in spectrum sensing phase the outcome of the binary detector is $\hat{\mathcal{H}}_{0,n}$. During this phase, SU_n sends Gaussian data symbols to the AP, while it adapts its transmission power according to information provided by the AP through the feedback channel about SU_n -AP link as well as its battery state. In particular, SU_n transmits N_d zero-mean i.i.d. complex Gaussian symbols $x_n[m]$ for $m = 1, \dots, N_d$ with power $P_{k,n} = \alpha_{k,n} p_u$, when the battery is at state k and $\alpha_{k,n}$ is given in (2). Let $s_n[m]$ denote the discrete-time representation of received signal at the AP from SU_n . Due to error in spectrum sensing, we need to distinguish the signal model for $s_n[m]$ under \mathcal{H}_0 and \mathcal{H}_1 . We have

$$\begin{aligned} \mathcal{H}_0, \hat{\mathcal{H}}_{0,n}: \quad s_n[m] &= h_n x_n[m] + v_n[m], \\ \mathcal{H}_1, \hat{\mathcal{H}}_{0,n}: \quad s_n[m] &= h_n x_n[m] + q[m] p[m] + v_n[m]. \end{aligned} \quad (25)$$

Substituting $h_n = \hat{h}_n + \tilde{h}_n$ in (25), we reach at

$$\begin{aligned} \mathcal{H}_0, \hat{\mathcal{H}}_{0,n}: \quad s_n[m] &= \hat{h}_n x_n[m] + \overbrace{\tilde{h}_n x_n[m]}^{\text{new noise } \eta_{n,0}[m]} + v_n[m], \\ \mathcal{H}_1, \hat{\mathcal{H}}_{0,n}: \quad s_n[m] &= \hat{h}_n x_n[m] + \overbrace{\tilde{h}_n x_n[m] + q[m] p[m]}^{\text{new noise } \eta_{n,1}[m]} + v_n[m], \end{aligned} \quad (26)$$

where the new noise terms depend on \tilde{h}_n . Given \hat{g}_n at the AP, we obtain an achievable rate expression for a time slot by considering symbol-wise mutual information between channel input and output over the duration of N_d data symbols as follows

$$\begin{aligned} R_n &= \frac{W D_d}{N_d} \sum_{m=1}^{N_d} \left[\beta_{0,n} \mathbb{E} \left\{ I(x_n[m]; s_n[m] | \hat{g}_n, \mathcal{H}_0, \hat{\mathcal{H}}_{0,n}) \right\} \right. \\ &\quad \left. + \beta_{1,n} \mathbb{E} \left\{ I(x_n[m]; s_n[m] | \hat{g}_n, \mathcal{H}_1, \hat{\mathcal{H}}_{0,n}) \right\} \right], \end{aligned} \quad (27)$$

where $D_d = \tau_d / T_f$ is the fraction of the time slot used for data transmission and the expectations in (27) are taken over the conditional probability density functions (pdfs) of \hat{g}_n given $\{\mathcal{H}_\varepsilon, \hat{\mathcal{H}}_{0,n}\}$ for $\varepsilon = 0, 1$. To characterize R_n in (27) we need to find $\mathbb{E}\{I(x_n[m]; s_n[m] | \hat{g}_n, \mathcal{H}_\varepsilon, \hat{\mathcal{H}}_{0,n})\}$. Exploiting the chain rule we can rewrite this expectation as follows

$$\begin{aligned} &\mathbb{E} \left\{ I(x_n[m]; s_n[m] | \hat{g}_n, \mathcal{H}_\varepsilon, \hat{\mathcal{H}}_{0,n}) \right\} \\ &= \sum_{k=0}^K \zeta_{k,n} I(x_n[m]; s_n[m] | \hat{g}_n, k, \mathcal{H}_\varepsilon, \hat{\mathcal{H}}_{0,n}). \end{aligned} \quad (28)$$

Note that $I(x_n[m]; s_n[m] | \hat{g}_n, \mathcal{H}_\varepsilon, \hat{\mathcal{H}}_{0,n})$ in (28) is the mutual information between $x_n[m]$ and $s_n[m]$ when the battery state is k , given \hat{g}_n and $\{\mathcal{H}_\varepsilon, \hat{\mathcal{H}}_{0,n}\}$. From now on, we drop the variable m in $x_n[m]$ and $s_n[m]$ for brevity of the presentation. Focusing on $I(x_n; s_n | \hat{g}_n, \mathcal{H}_\varepsilon, \hat{\mathcal{H}}_{0,n})$, we have

$$\begin{aligned} I(x_n; s_n | \hat{g}_n, k, \mathcal{H}_\varepsilon, \hat{\mathcal{H}}_{0,n}) &= h(x_n | \hat{g}_n, k, \hat{\mathcal{H}}_{0,n}, \mathcal{H}_\varepsilon) \\ &\quad - h(x_n | s_n, \hat{g}_n, k, \hat{\mathcal{H}}_{0,n}, \mathcal{H}_\varepsilon), \end{aligned} \quad (29)$$

where $h(\cdot)$ is the differential entropy. Consider the first term in (29). Since $x_n \sim \mathcal{CN}(0, P_{k,n})$ we have $h(x_n | \hat{g}_n, k, \hat{\mathcal{H}}_{0,n}, \mathcal{H}_\varepsilon) = \log_2(\pi e P_{k,n})$. Consider the second term in (29). Due to channel estimation error, the new noises $\eta_{n,\varepsilon}$'s in (26) are non-Gaussian and this term does not have a closed form expression. Hence, similar to [34], [38], [45] we employ bounding techniques to find an upper bound on this term. This term is upper bounded by the entropy of a Gaussian random variable with the variance $\Theta_M^{n,\varepsilon}$

$$\Theta_M^{n,\varepsilon} = \mathbb{E} \left\{ |x_n - \mathbb{E}\{x_n | \hat{g}_n, k, \hat{\mathcal{H}}_{0,n}, \mathcal{H}_\varepsilon\}|^2 \right\}, \quad (30)$$

where the expectations are taken over the conditional pdf of x_n given $s_n, \hat{g}_n, k, \hat{\mathcal{H}}_{0,n}, \mathcal{H}_\varepsilon$. In fact, $\Theta_M^{i,\varepsilon}$ is the mean square error (MSE) of the MMSE estimate of x_n given $s_n, \hat{g}_n, k, \hat{\mathcal{H}}_{0,n}, \mathcal{H}_\varepsilon$. Using minimum variance property of MMSE estimator, we have $\Theta_M^{n,\varepsilon} \leq \Theta_L^{n,\varepsilon}$, where $\Theta_L^{n,\varepsilon}$ is the MSE of the LMMSE estimate of x_n given $s_n, \hat{g}_n, k, \hat{\mathcal{H}}_{0,n}, \mathcal{H}_\varepsilon$. Combining all, we find $h(x_n | s_n, \hat{g}_n, k, \hat{\mathcal{H}}_{0,n}, \mathcal{H}_\varepsilon) \leq \log_2(\pi e \Theta_L^{n,\varepsilon})$ and $I(x_n; s_n | \hat{g}_n, k, \hat{\mathcal{H}}_{0,n}, \mathcal{H}_\varepsilon) \geq \log_2(P_{k,n} / \Theta_L^{n,\varepsilon})$ where

$$\Theta_L^{n,\varepsilon} = \frac{P_{k,n} \sigma_{\eta_{n,\varepsilon}}^2}{\sigma_{\eta_{n,\varepsilon}}^2 + \hat{g}_n P_{k,n}}, \quad (31)$$

$$\sigma_{\eta_{n,\varepsilon}}^2 = \tilde{\gamma}_n^\varepsilon P_{k,n} + \sigma_{v_n}^2 + \varepsilon \sigma_p^2. \quad (32)$$

At the end, we obtain the lower bounds as follow

$$I(x_n; s_n | \hat{g}_n, k, \hat{\mathcal{H}}_{0,n}, \mathcal{H}_0) \geq \log_2(1 + \hat{g}_n b_{k,n}^0), \quad (33a)$$

$$I(x_n; s_n | \hat{g}_n, k, \hat{\mathcal{H}}_{0,n}, \mathcal{H}_1) \geq \log_2(1 + \hat{g}_n b_{k,n}^1), \quad (33b)$$

where

$$b_{k,n}^0 = \frac{P_{k,n}}{(\tilde{\gamma}_n^0 P_{k,n} + \sigma_{v_n}^2)}, \quad b_{k,n}^1 = \frac{P_{k,n}}{(\tilde{\gamma}_n^1 P_{k,n} + \sigma_{v_n}^2 + \sigma_p^2)}. \quad (34)$$

Substituting equations (28) and (33) in (27) and noting that the symbol-wise mutual information between channel input and output for N_d data symbols are equal we reach at

$$\begin{aligned} R_n &\geq R_{n, \text{LB}} = D_d \beta_{0,n} W \sum_{k=0}^K \zeta_{k,n} \mathbb{E} \left\{ \log_2(1 + \hat{g}_n b_{k,n}^0) | \mathcal{H}_0 \right\} \\ &\quad + D_d \beta_{1,n} W \sum_{k=0}^K \zeta_{k,n} \mathbb{E} \left\{ \log_2(1 + \hat{g}_n b_{k,n}^1) | \mathcal{H}_1 \right\}. \end{aligned} \quad (35)$$

Next, we compute the conditional expectations in (35), in which we take average over \hat{g}_n , given \mathcal{H}_ε . Using (3) and (4c) we have

$$\begin{aligned} \mathbb{E}\left\{\log_2(1+\hat{g}_n b_{k,n}^\varepsilon)|\mathcal{H}_\varepsilon\right\} &= \sum_{i=1}^{\lfloor k\Omega_n \rfloor - \alpha_t} \int_{a_{i,k,n}}^{c_{i,k,n}} \log_2(1+S_{i,n}^\varepsilon x) f_{\hat{g}_n}^\varepsilon(x) dx \\ &= \sum_{i=1}^{\lfloor k\Omega_n \rfloor - \alpha_t} V_k(S_{i,n}^\varepsilon, \hat{\gamma}_n^\varepsilon) \end{aligned} \quad (36a)$$

in which

$$S_{i,n}^0 = \frac{i p_u}{(\tilde{\gamma}_n^0 i p_u + \sigma_v^2)}, \quad S_{i,n}^1 = \frac{i p_u}{(\tilde{\gamma}_n^1 i p_u + \sigma_v^2 + \sigma_p^2)}, \quad (36b)$$

$$V_k(S_{i,n}, \hat{\gamma}_n) = M(c_{i,k,n}, S_{i,n}, \hat{\gamma}_n) - M(a_{i,k,n}, S_{i,n}, \hat{\gamma}_n), \quad (36c)$$

and

$$\begin{aligned} M(x, S, w) &= \int \log_2(1+Sx) \frac{e^{-\frac{x}{w}}}{w} dx \\ &= \frac{e^{\frac{1}{Sw}}}{\ln(2)} \text{Ei}\left(\frac{-x}{w} - \frac{1}{Sw}\right) - e^{-\frac{x}{w}} \log_2(1+Sx). \end{aligned} \quad (37)$$

Also, $c_{i,k,n}$ and $a_{i,k,n}$ are given in (4c). Substituting (36a) in (35) we reach to

$$\begin{aligned} R_{n,\text{LB}} &= D_d \beta_{0,n} W \sum_{k=\alpha_t+1}^K \sum_{i=1}^{\lfloor k\Omega_n \rfloor - \alpha_t} \zeta_{k,n} V_k(S_{i,n}^0, \hat{\gamma}_n^0) \\ &\quad + D_d \beta_{1,n} W \sum_{k=\alpha_t+1}^K \sum_{i=1}^{\lfloor k\Omega_n \rfloor - \alpha_t} \zeta_{k,n} V_k(S_{i,n}^1, \hat{\gamma}_n^1). \end{aligned} \quad (38)$$

We note that the lower bounds in (33) are achieved when the new noises $\eta_{n,0}, \eta_{n,1}$ in (26) are regarded as worst-case Gaussian noise and hence the MMSE and LMMSE of x_n given $s_n, \hat{g}_n, k, \hat{\mathcal{H}}_{0,n}, \mathcal{H}_\varepsilon$ coincide. Given the rate lower bound $R_{n,\text{LB}}$ for SU_n , the sum-rate lower bound for all SU_n 's is

$$R_{\text{LB}} = \sum_{n=1}^{N_u} R_{n,\text{LB}}. \quad (39)$$

So far, we have established a sum-rate lower bound on the achievable sum-rate. Next, we characterize the average interference constraint (AIC). Suppose \bar{I}_{av} is the maximum allowed average interference power, i.e., the average interference power that collective SUs impose on PU_{rx} cannot exceed \bar{I}_{av} . To satisfy AIC, we have

$$\sum_{n=1}^{N_u} \beta_{1,n} \mathbb{E}\{z_n\} \left[D_d \mathbb{E}\{P_n(\hat{g}_n)\} + D_t P_t \right] \leq \bar{I}_{\text{av}}, \quad (40)$$

where $D_t = \tau_t/T_f$ and the expectation is over the conditional pdfs of \hat{g}_n under $\{\mathcal{H}_1, \hat{\mathcal{H}}_{0,n}\}$. The first term in (40) is the average interference power imposed on PU_{rx} when SUs transmit data symbols, and the second term is the average interference imposed on PU_{rx} when SUs send training symbols for channel estimation at the AP. Using (3) we compute the

term with expectation inside (40) as follows

$$\begin{aligned} \mathbb{E}\{P_n(\hat{g}_n)\} &= \sum_{k=0}^K \zeta_{k,n} \sum_{i=0}^K \Pr(\alpha_{k,n} = i | \mathcal{H}_1) i p_u \\ &= \sum_{k=\alpha_t+1}^K \zeta_{k,n} \sum_{i=1}^{\lfloor k\Omega_n \rfloor - \alpha_t} \psi_{i,k,n}^1 i p_u. \end{aligned} \quad (41)$$

Substituting (41) into (40), we can rewrite the AIC in (40) as

$$\sum_{n=1}^{N_u} \beta_{1,n} \delta_{z_n} \left[\sum_{k=\alpha_t+1}^K \zeta_{k,n} \sum_{i=1}^{\lfloor k\Omega_n \rfloor - \alpha_t} \psi_{i,k,n}^1 i p_u + D_t P_t \right] \leq \bar{I}_{\text{av}}. \quad (42)$$

For ideal spectrum sensing we get $\beta_{1,n} = 0$ in (15), implying that data transmission from SUs to the AP does not cause interference on PU_{rx} and the left-hand side of (42) becomes zero, i.e., the AIC is always satisfied.

Next, we examine how spectrum sensing error and channel estimation error affect R_{LB} and AIC expressions. First, spectrum sensing error affects AIC via $\beta_{1,n}$, and R_{LB} via $\beta_{0,n}$ and $\beta_{1,n}$. Recall $\beta_{0,n}, \beta_{1,n}$ depend on $\pi_0, P_{\text{fa},n}, P_{\text{d},n}$ (see (15)). Second, channel estimation error affects AIC via $D_t, \psi_{i,k,n}^1$, and R_{LB} via $\tilde{\gamma}_n^\varepsilon$.

Having the mathematical expressions for R_{LB} and AIC, our goal is to optimize the set of transmission parameters $\{\Omega_n, \theta_n\}$ for all SUs such that R_{LB} is maximized, subject to the AIC. To inspect the underlying trade-offs between decreasing the average interference power imposed by SU_n 's on PU_{rx} and increasing the sum-rate lower bound R_{LB} , we note that increasing data symbol transmission power $P_{k,n}$ increases R_{LB} . However, it increases the average interference power. Aiming to strike a balance between increasing R_{LB} and decreasing the imposed average interference power, we seek the optimal $\{\Omega_n, \theta_n\}_{n=1}^{N_u}$ such that R_{LB} in (35) is maximized, subject to AIC given in (42). In other words, we are interested in solving the following constrained optimization problem

$$\begin{aligned} \text{(P1)} \quad & \text{Maximize } R_{\text{LB}} \\ & \{\Omega_n, \theta_n\}_{n=1}^{N_u} \\ \text{s.t.: } & \Omega_n \in [0, 1], \\ & \theta_n \geq 0, \\ & \text{AIC in (42) is satisfied.} \end{aligned}$$

We note that solving (P1) requires an $2N_u$ -dimensional search over the search space $[0, 1]^{N_u} \times [0, \infty)^{N_u}$.

VI. SIMULATION RESULTS

In this section we corroborate our analysis on constrained maximization of the achievable sum-rate lower bound with Matlab simulations, and examine how the optimized sum-rate lower bound depends on the average number of harvesting energy packets ρ_n , the maximum allowed average interference power \bar{I}_{av} , the duration of spectrum sensing phase τ_s , the number of consumed cells of energy for channel probing α_t , and the size of the battery K . Our simulation parameters are given in Table II.

• **Spectrum sensing-channel probing-data transmission trade-offs:** To explore these trade-offs, in this section we let $N_u = 1$ and examine how the rate lower bound R_{LB} in (39) for

TABLE II: Simulation Parameters

Parameter	Value	Parameter	Value
P_p	1 watts	$\sigma_{v_n}^2$	1
π_0	0.7	$\sigma_{w_n}^2$	1
τ_t	0.1 ms	α_t	1
τ_s	1 ms	\bar{P}_d	0.85
T_f	10 ms	W	10 KHz
e_u	0.01	δ_q	1

a single user changes when we vary τ_s , or α_t . The simulation parameters, except for $\alpha_t, \tau_s, \sigma_w^2, \sigma_v^2$ are given in Table II ³.

Fig. 5a shows R_{LB} versus τ_s for two values of the energy harvesting parameter $\rho = 15, 16, \sigma_w^2 = \sigma_v^2 = 1$ and $\alpha_t = 1$. This figure suggests that there exists a trade-off between τ_s and R_{LB} . On the positive side, as τ_s (or equivalently N_s) increases, the accuracy of the energy detector for spectrum sensing increases (i.e., P_{fa_n} in (13b) decreases). A more accurate spectrum sensing can reveal new opportunities for SU_n to be exploited for its data transmission, that can increase R_{LB} . On the negative side, as τ_s increases, the duration of data transmission phase $\tau_d = T_f - \tau_s - \tau_t$ decreases. This trade-off between spectrum sensing and data transmission indicates that, given the parameters (including α_t), there is an optimal τ_s , denoted as τ_s^* in Fig. 5a, that maximizes R_{LB} . For instance, for $\rho = 15, 16$ we have $\tau_s^* = 0.6, 0.75$ ms.

Fig. 5b plots R_{LB} versus α_t for $\rho = 18, 20, \tau_s = 1$ ms and $\sigma_w^2 = \sigma_v^2 = 5$. This figure suggests that a trade-off exists between α_t and R_{LB} . On the positive side, as α_t increases, the accuracy of channel probing (measured by the variance of channel estimation error in (21)) improves. A more accurate channel probing can increase R_{LB} . On the negative side, as α_t increases, the available energy for data transmission decreases. This trade-off between channel probing and data transmission shows that, given the parameters (including τ_s), there is an optimal α_t , denoted as α_t^* in Fig. 5b, that maximizes R_{LB} . For instance, for $\rho = 15, 16$ we have $\alpha_t^* = 4$.

• **Effect of the optimization variables Ω, θ :** In this section, we let $N_u = 1$ and we illustrate how the entries of the steady-state probability vector ζ in (10), R_{LB} in (39) for a single user, and the battery outage probability P_b^{out} defined below depend on the optimization variables Ω and θ . We define $P_{b_n}^{\text{out}}$ as the steady-state probability of the battery of SU_n being equal or lower than α_t . When the battery is at outage, it cannot yield energy for data transmission or channel probing. We have

$$P_{b_n}^{\text{out}} = \Pr(\mathcal{B}_n \leq \alpha_t) = \sum_{k=0}^{\alpha_t} \zeta_{k,n}. \quad (43)$$

The simulation parameters are given in Table II. Also, we let $\gamma = 2, \delta_u = 1, \delta_z = 1$.

Fig. 6a illustrates R_{LB} for a single user versus Ω for $\rho = 15, 20$. We observe that R_{LB} is neither a convex nor a concave function of Ω . This figure suggests that there is an optimal Ω , which we denote as Ω^* , that maximizes R_{LB} . Starting from small values of Ω , as Ω increases (until it reaches

³Note that the variances of channel estimate and corresponding estimation error in (21) depend on the product $P_t N_t = \alpha_t e_u f_s$ and is independent of τ_t . That is the reason, instead of τ_t , we consider varying α_t , to understand channel probing trade-offs.

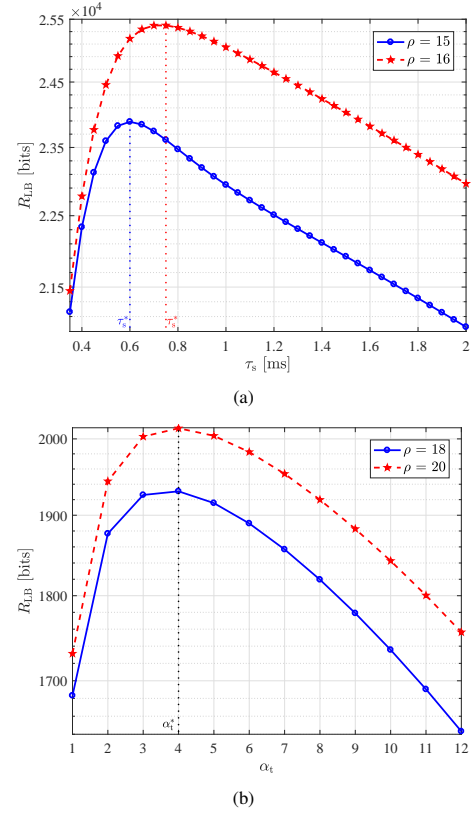


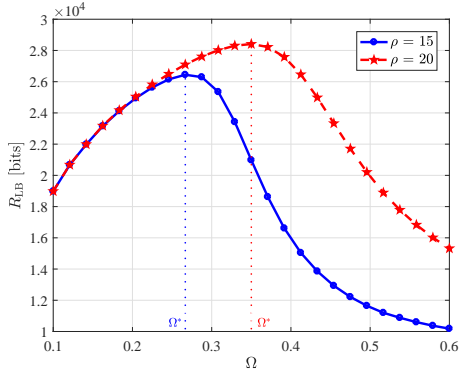
Fig. 5: (a) R_{LB} versus τ_s for $K = 80, \theta = 0.25, \Omega = 0.35, \sigma_w^2 = \sigma_v^2 = 1$, (b) R_{LB} versus α_t for $K = 200, \theta = 0.25, \Omega = 0.35, \sigma_w^2 = \sigma_v^2 = 5$.

the value Ω^*), R_{LB} increases, because the harvested energy can recharge the battery and can yield more power for data transmission. However, when Ω exceeds Ω^* , the harvested and stored energy cannot support the data transmission and R_{LB} decreases. Moreover, as ρ increases, R_{LB} increases as well. The behavior of R_{LB} versus θ is shown in Fig. 6b for $\rho = 15, 18$. We observe that R_{LB} is neither a convex nor a concave function of θ . Similar to Ω , there is an optimal θ , which we denote as θ^* , that maximizes R_{LB} . Starting from small values of θ , as θ increases (until it reaches θ^*), R_{LB} increases. However, when θ exceeds θ^* , R_{LB} decreases.

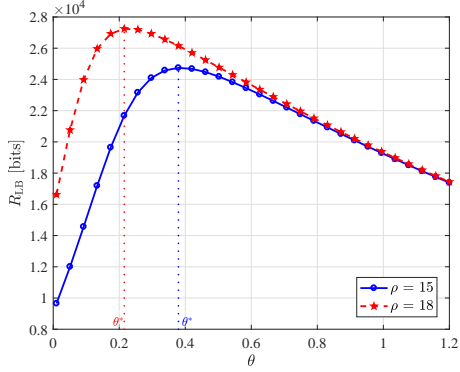
Fig. 7 plots the entries of the steady-state probability vector ζ versus k for $\Omega = 0.45, 0.3$ and $\theta = 0.2$. Fig. 8 plots the entries of ζ versus k for $\theta = 0.1, 0.5$ and $\Omega = 0.35$. To quantify the effect of Ω and θ on the entries of ζ we define the average energy stored at the battery of SU_n as

$$\bar{\mathcal{B}}_n = \mathbb{E}\{\mathcal{B}_n\} = \sum_{k=0}^K k \zeta_{k,n}, \quad (44)$$

where the largest possible value for $\bar{\mathcal{B}}_n$ is K . Considering Figs. 7a and 7b, we find $\bar{\mathcal{B}}_n^{(a)} = 16.97$ for $\Omega = 0.45$ (the battery is near empty) and $\bar{\mathcal{B}}_n^{(b)} = 66.30$ for $\Omega = 0.30$ (the battery is near full). Considering Figs. 8a and 8b, we find $\bar{\mathcal{B}}_n^{(a)} = 24.08$ for $\theta = 0.1$ and $\bar{\mathcal{B}}_n^{(b)} = 71.55$ for $\theta = 0.5$. Clearly, the values of Ω and θ affect $\bar{\mathcal{B}}$. Given θ , when Ω is large, data transmit energy α_k in (2) is large. Due to large energy consumption for data transmission (compared to energy



(a)

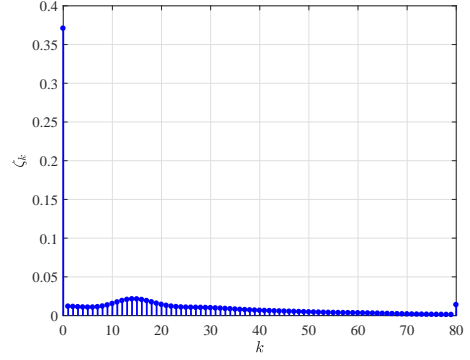


(b)

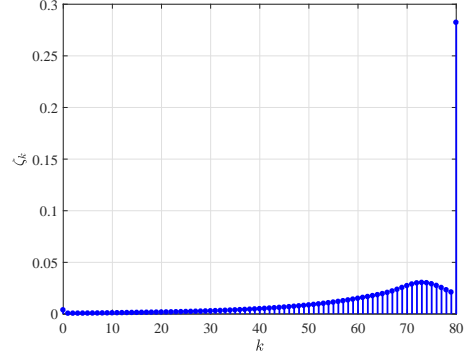
Fig. 6: (a) R_{LB} versus Ω for $K = 80, \theta = 0.2$, (b) R_{LB} versus θ for $K = 80, \Omega = 0.35$.

harvesting) the battery becomes near empty at its steady-state and SU may stop functioning, due to energy outage. When Ω is small, α_k in (2) is small. Due to small energy consumption for data transmission (compared to energy harvesting) the battery becomes near full at its steady-state, indicating that SU has failed to utilize the excess energy. Both cases inevitably hinder data transmission, leading to a reduction in R_{LB} . Similar argument holds true, when θ varies and Ω is given. In particular, when θ is small, transmit energy α_k in (2) is large, and when θ is large, transmit energy α_k in (2) is small. Again, both cases impede data transmission, leading to a lower R_{LB} . Overall, the observations we make in Figs. 6, 7, 8 confirm that optimizing both Ω and θ to achieve a balance between the energy harvesting and the energy consumption for data transmission is of high importance.

Fig. 9a illustrates the behavior of P_b^{Out} for a single user in terms of Ω for $\theta = 0.05$. Fig. 9b plots P_b^{Out} versus θ for $\Omega = 0.35$. For $\alpha_t = 1$, P_b^{Out} in (43) reduces to $P_b^{Out} = \zeta_0 + \zeta_1$, i.e., P_b^{Out} depends on Ω and θ , via only the first two entries of vector ζ . Fig. 9a shows that, as Ω increases, P_b^{Out} increases as well. This is because as Ω increases, given θ , α_k in (2) increases. Due to large energy consumption for data transmission the chance of the battery depletion and hence P_b^{Out} increase. Fig. 9b demonstrates that, as θ increases, P_b^{Out} decreases. This is because as θ increases, given Ω , α_k in (2) decreases. Due to small energy consumption for data transmission the chance of the battery depletion and hence P_b^{Out} decrease.

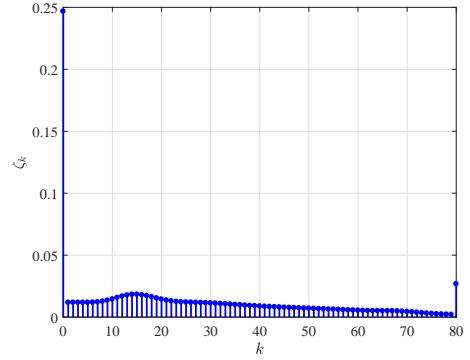


(a)

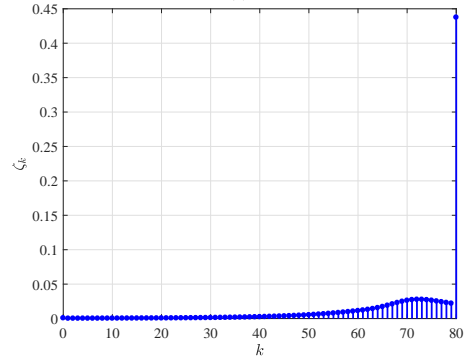


(b)

Fig. 7: ζ_k versus k for $K = 80, \rho = 15, \theta = 0.2$, (a) $\Omega = 0.45$, (b) $\Omega = 0.30$.



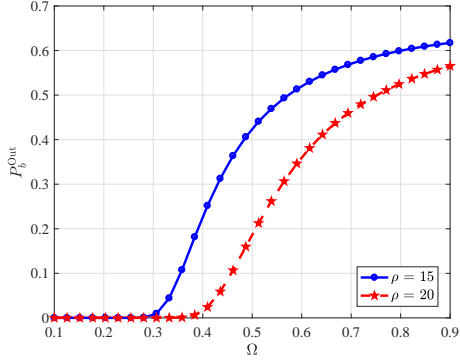
(a)



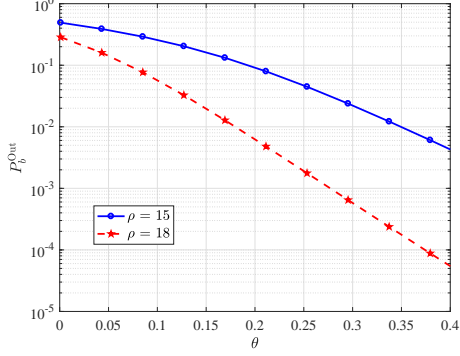
(b)

Fig. 8: ζ_k versus k for $K = 80, \rho = 15, \Omega = 0.35$, (a) $\theta = 0.1$, (b) $\theta = 0.5$.

• **Solving Problem (P1):** Next, we consider solving the constrained optimization problem (P1) and plot the maximized R_{LB} , denoted as R_{LB}^* (R_{LB}^* is R_{LB} evaluated at the solutions



(a)



(b)

Fig. 9: (a) P_b^{Out} versus Ω for $K = 80, \theta = 0.05$, (b) P_b^{Out} versus θ for $K = 80, \Omega = 0.35$.

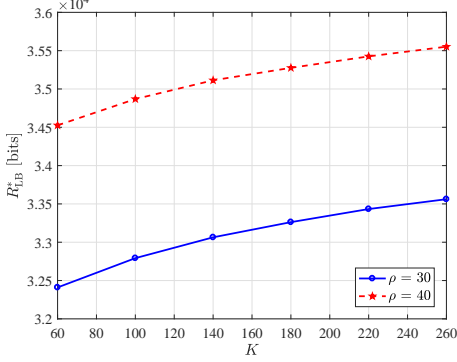


Fig. 10: R_{LB}^* versus K for $\bar{T}_{\text{av}} = 2$ dB.

obtained from solving (P1)).

Fig. 10 depicts R_{LB}^* versus K for $N_u = 3$. We let the statistics of fading coefficients be different across SUs, $\gamma = [2, 2.2, 2.1]$, $\delta_u = [1, 0.8, 1.2]$, $\delta_z = [1, 0.5, 0.8]$ and $\rho = 30, 40$ be equal for all SUs. We observe that as K increases, R_{LB}^* increases. This is expected, since as K increases the chance of energy overflow decreases, leading to a larger amount of stored energy in the battery, which can be utilized to support a higher data rate transmission.

Fig. 11 shows R_{LB}^* versus \bar{T}_{av} for $K = 80, \rho = 10, 15$ and $N_u = 3$. For small \bar{T}_{av} , the AIC in (42) is active and consequently, it limits transmit power of SUs. As \bar{T}_{av} increases, SUs can transmit at higher power levels and R_{LB}^* increases, until R_{LB}^* reaches its maximum value. Increasing \bar{T}_{av} any further, beyond the knee point in Fig. 11, does

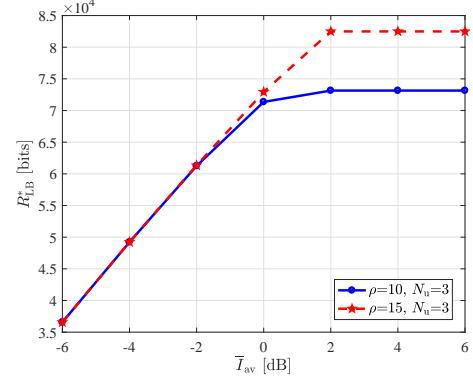


Fig. 11: R_{LB}^* versus \bar{T}_{av} for $N_u = 3, K = 80$.

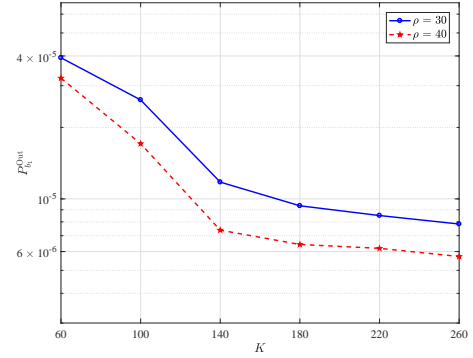


Fig. 12: $P_{b_1}^{\text{Out}}$ for SU_1 versus K when $\bar{T}_{\text{av}} = 2$ dB.

not increase R_{LB}^* . This is because for large \bar{T}_{av} , transmit power levels are restricted by the amount of harvested and stored energy in the battery (and not by the AIC). Therefore, increasing \bar{T}_{av} beyond the knee point has no effect on R_{LB}^* . Moreover, for small \bar{T}_{av} where the AIC is active, increasing ρ has no effect on R_{LB}^* . On the other hand, for large \bar{T}_{av} , when ρ increases, R_{LB}^* increases.

Considering SU_1 , Fig 12 depicts $P_{b_1}^{\text{Out}}$ of this user versus K where the optimization variables Ω_1 and θ_1 are obtained by solving (P1) and maximizing R_{LB} and then substituting the optimized variables in (43) to calculate $P_{b_1}^{\text{Out}}$. We observe that increasing K leads to a lower $P_{b_1}^{\text{Out}}$.

We define the transmission outage probability $P_{\alpha_n}^{\text{Out}}$ as the probability of SU_n not being able to transmit data to the AP (due to either a weak SU_n -AP link with small fading coefficient or insufficient amount of stored energy at the battery). We have

$$P_{\alpha_n}^{\text{Out}} = \Pr(P_n = 0 | \hat{\mathcal{H}}_{0,n}) = \omega_{0,n} \Pr(P_n = 0 | \hat{\mathcal{H}}_{0,n}, \mathcal{H}_0) + \omega_{1,n} \Pr(P_n = 0 | \hat{\mathcal{H}}_{0,n}, \mathcal{H}_1), \quad (45)$$

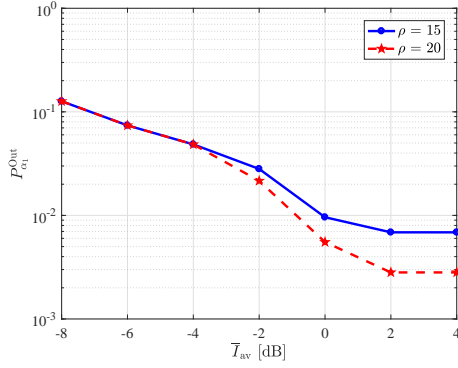


Fig. 13: $P_{\alpha_1}^{\text{Out}}$ for SU_1 versus \bar{T}_{av} for SU_1 when $K = 100$.

where

$$\begin{aligned} & \Pr(P_n = 0 | \hat{\mathcal{H}}_{0,n}, \mathcal{H}_\varepsilon) \\ &= \sum_{k=0}^{\alpha_t} \zeta_{k,n} \Pr(\alpha_{k,n} = 0 | \hat{\mathcal{H}}_{0,n}, \mathcal{H}_\varepsilon, \mathcal{B}_n \leq \alpha_t) \\ &+ \sum_{k=\alpha_t+1}^K \zeta_{k,n} \Pr(\alpha_{k,n} = 0 | \hat{\mathcal{H}}_{0,n}, \mathcal{H}_\varepsilon, \mathcal{B}_n \geq \alpha_t + 1). \end{aligned} \quad (46)$$

Substituting (3) and (46) in (45) we get

$$P_{\alpha_n}^{\text{Out}} = \sum_{k=0}^{\alpha_t} \zeta_{k,n} + \sum_{k=\alpha_t+1}^K \zeta_{k,n} Y_{k,n}. \quad (47)$$

Fig. 13 shows $P_{\alpha_1}^{\text{Out}}$ for SU_1 versus \bar{T}_{av} where the optimization variables Ω_1 and θ_1 are obtained by solving (P1) and maximizing R_{LB} and then substituting the optimized variables in (47) to compute $P_{\alpha_1}^{\text{Out}}$. Starting from small \bar{T}_{av} , as \bar{T}_{av} increases, SUs can transmit at higher power levels and $P_{\alpha_1}^{\text{Out}}$ decreases, until $P_{\alpha_1}^{\text{Out}}$ reaches its minimum value. Increasing \bar{T}_{av} any further, beyond the knee point in Fig. 13, does not reduce $P_{\alpha_1}^{\text{Out}}$. This is because for large \bar{T}_{av} transmit power levels are restricted by the amount of harvested and stored energy in the battery (and not by the AIC). Therefore, increasing \bar{T}_{av} beyond the knee point has no effect on $P_{\alpha_1}^{\text{Out}}$.

VII. CONCLUSION

We considered an opportunistic CR network, consisting of N_u SUs and the AP, that can access a spectrum band licensed to a primary network. Each SU is capable of harvesting energy from ambient energy sources, and is equipped with a finite size battery, for storing its harvested energy. The SUs operate under a time-slotted scheme, where each time slot consists of: spectrum sensing phase, channel probing phase, and data transmission phase. To achieve a balance between the energy harvesting and the energy consumption, we proposed a parametrized power control strategy that allows each SU to adapt its power, according to the received feedback information from the AP regarding its link fading coefficient and its stored energy in the battery. Modeling the randomly arriving energy packets during a time slot as a Poisson process, and the dynamics of the battery as a finite state Markov chain, we established a lower bound on the achievable sum-rate of SUs-AP links, in the presence of both spectrum sensing and

channel estimation errors. We optimized the parameters of the proposed power control strategy, such that the derived sum-rate lower bound is maximized, subject to the AIC. We validated our analysis via Matlab simulations and explored spectrum sensing-channel probing-data transmission trade-offs. We also illustrated how the AIC, the harvesting parameter, and the battery size impact the sum-rate, as well as transmission outage probability.

REFERENCES

- [1] T. Yucek and H. Arslan, "A survey of spectrum sensing algorithms for cognitive radio applications," *IEEE Communications Surveys Tutorials*, vol. 11, no. 1, pp. 116–130, First 2009.
- [2] A. Ali and W. Hamouda, "Advances on spectrum sensing for cognitive radio networks: Theory and applications," *IEEE Communications Surveys Tutorials*, vol. 19, no. 2, pp. 1277–1304, 2017.
- [3] S. Stotas and A. Nallanathan, "Optimal sensing time and power allocation in multiband cognitive radio networks," *IEEE Transactions on Communications*, vol. 59, no. 1, pp. 226–235, January 2011.
- [4] H. Yazdani and A. Vosoughi, "On the spectrum sensing, beam selection and power allocation in cognitive radio networks using reconfigurable antennas," in *2019 53rd Annual Conference on Information Sciences and Systems (CISS)*, March 2019.
- [5] H. Yazdani, A. Vosoughi, and X. Gong, "Beam selection and discrete power allocation in opportunistic cognitive radio systems with limited feedback using ESPAR antennas," *IEEE Transactions on Cognitive Communications and Networking*, vol. 6, no. 1, pp. 325–339, 2020.
- [6] H. Yazdani, A. Vosoughi, and X. Gong, "Achievable rates of opportunistic cognitive radio systems using reconfigurable antennas with imperfect sensing and channel estimation," *arXiv:2007.04390*, 2020.
- [7] S. Mao, M. H. Cheung, and V. W. S. Wong, "Joint energy allocation for sensing and transmission in rechargeable wireless sensor networks," *IEEE Transactions on Vehicular Technology*, vol. 63, no. 6, pp. 2862–2875, 2014.
- [8] S. Yin, Z. Qu, and S. Li, "Achievable throughput optimization in energy harvesting cognitive radio systems," *IEEE Journal on Selected Areas in Communications*, vol. 33, no. 3, pp. 407–422, 2015.
- [9] S. Biswas, S. Dey, and A. Shirazinia, "Sum throughput maximization in a cognitive multiple access channel with cooperative spectrum sensing and energy harvesting," *IEEE Transactions on Cognitive Communications and Networking*, vol. 5, no. 2, pp. 382–399, 2019.
- [10] M. Ku, W. Li, Y. Chen, and K. J. Ray Liu, "Advances in energy harvesting communications: Past, present, and future challenges," *IEEE Communications Surveys Tutorials*, vol. 18, no. 2, pp. 1384–1412, 2016.
- [11] H. Zhang, Y. Nie, J. Cheng, V. C. M. Leung, and A. Nallanathan, "Sensing time optimization and power control for energy efficient cognitive small cell with imperfect hybrid spectrum sensing," *IEEE Transactions on Wireless Communications*, vol. 16, no. 2, pp. 730–743, Feb 2017.
- [12] L. Zhang, M. Xiao, G. Wu, S. Li, and Y. Liang, "Energy-efficient cognitive transmission with imperfect spectrum sensing," *IEEE Journal on Selected Areas in Communications*, vol. 34, no. 5, pp. 1320–1335, 2016.
- [13] K. Wu, H. Jiang, and C. Tellambura, "Sensing, probing, and transmitting strategy for energy harvesting cognitive radio," in *2017 IEEE International Conference on Communications (ICC)*, May 2017, pp. 1–6.
- [14] W. Chung, S. Park, S. Lim, and D. Hong, "Optimal transmit power control for energy-harvesting cognitive radio system," in *2013 IEEE 78th Vehicular Technology Conference (VTC Fall)*, Sep. 2013, pp. 1–5.
- [15] A. Sultan, "Sensing and transmit energy optimization for an energy harvesting cognitive radio," *IEEE Wireless Communications Letters*, vol. 1, no. 5, pp. 500–503, October 2012.
- [16] F. Zhang, T. Jing, Y. Huo, and K. Jiang, "Throughput maximization for energy harvesting cognitive radio networks with finite horizon," in *2017 9th International Conference on Wireless Communications and Signal Processing (WCSP)*, Oct 2017, pp. 1–7.
- [17] G. Ardeshiri, H. Yazdani, and A. Vosoughi, "Optimal local thresholds for distributed detection in energy harvesting wireless sensor networks," in *2018 IEEE Global Conference on Signal and Information Processing (GlobalSIP)*, Nov 2018, pp. 813–817.
- [18] —, "Power adaptation for distributed detection in energy harvesting WSNs with finite-capacity battery," in *2019 IEEE Global Communications Conference (GLOBECOM)*, 2019, pp. 1–6.

- [19] S. Park, H. Kim, and D. Hong, "Cognitive radio networks with energy harvesting," *IEEE Transactions on Wireless Communications*, vol. 12, no. 3, pp. 1386–1397, March 2013.
- [20] S. Park and D. Hong, "Achievable throughput of energy harvesting cognitive radio networks," *IEEE Transactions on Wireless Communications*, vol. 13, no. 2, pp. 1010–1022, February 2014.
- [21] D. Zhang, Z. Chen, J. Ren, N. Zhang, M. K. Awad, H. Zhou, and X. S. Shen, "Energy-harvesting-aided spectrum sensing and data transmission in heterogeneous cognitive radio sensor network," *IEEE Transactions on Vehicular Technology*, vol. 66, no. 1, pp. 831–843, 2017.
- [22] H. S. Lee, M. E. Ahmed, and D. I. Kim, "Optimal spectrum sensing policy in RF-powered cognitive radio networks," *IEEE Transactions on Vehicular Technology*, vol. 67, no. 10, pp. 9557–9570, 2018.
- [23] D. Niyato, P. Wang, and D. I. Kim, "Performance analysis of cognitive radio networks with opportunistic RF energy harvesting," in *2014 IEEE Global Communications Conference*, 2014, pp. 1096–1101.
- [24] D. Altinel and G. K. Kurt, "Finite-state markov channel based modeling of RF energy harvesting systems," *IEEE Transactions on Vehicular Technology*, vol. 67, no. 2, pp. 1713–1725, 2018.
- [25] X. Yang, M. Sheng, H. Sun, X. Wang, and J. Li, "Spatial throughput analysis and transmission strategy design in energy harvesting cognitive radio networks," *IEEE Transactions on Communications*, vol. 66, no. 12, pp. 5938–5951, 2018.
- [26] S. Park, J. Heo, B. Kim, W. Chung, H. Wang, and D. Hong, "Optimal mode selection for cognitive radio sensor networks with RF energy harvesting," in *2012 IEEE 23rd International Symposium on Personal, Indoor and Mobile Radio Communications - (PIMRC)*, 2012, pp. 2155–2159.
- [27] J. Yan and Y. Liu, "A dynamic SWIPT approach for cooperative cognitive radio networks," *IEEE Transactions on Vehicular Technology*, vol. 66, no. 12, pp. 11 122–11 136, 2017.
- [28] F. Zhou, Z. Li, J. Cheng, Q. Li, and J. Si, "Robust AN-aided beamforming and power splitting design for secure MISO cognitive radio with SWIPT," *IEEE Transactions on Wireless Communications*, vol. 16, no. 4, pp. 2450–2464, 2017.
- [29] M. R. Zenaidi, Z. Rezk, and M. Alouini, "On communications under stochastic energy harvesting with noisy channel state information," in *2016 IEEE Global Communications Conference (GLOBECOM)*, 2016, pp. 1–6.
- [30] R. Ma and W. Zhang, "Optimal power allocation for energy harvesting communications with limited channel feedback," in *2014 IEEE Global Conference on Signal and Information Processing (GlobalSIP)*, 2014, pp. 193–197.
- [31] A. H. Sakr and E. Hossain, "Cognitive and energy harvesting-based D2D communication in cellular networks: Stochastic geometry modeling and analysis," *IEEE Transactions on Communications*, vol. 63, no. 5, pp. 1867–1880, 2015.
- [32] M. Ku, Y. Chen, and K. J. R. Liu, "Data-driven stochastic models and policies for energy harvesting sensor communications," *IEEE Journal on Selected Areas in Communications*, vol. 33, no. 8, pp. 1505–1520, 2015.
- [33] M. R. Zenaidi, Z. Rezk, and M. Alouini, "Performance limits of online energy harvesting communications with noisy channel state information at the transmitter," *IEEE Access*, vol. 5, pp. 1239–1249, 2017.
- [34] B. Hassibi and B. M. Hochwald, "How much training is needed in multiple-antenna wireless links?" *IEEE Transactions on Information Theory*, vol. 49, no. 4, pp. 951–963, April 2003.
- [35] M. Medard, "The effect upon channel capacity in wireless communications of perfect and imperfect knowledge of the channel," *IEEE Transactions on Information Theory*, vol. 46, no. 3, pp. 933–946, 2000.
- [36] M. Shirazi and A. Vosoughi, "On distributed estimation in hierarchical power constrained wireless sensor networks," *IEEE Transactions on Signal and Information Processing over Networks*, vol. 6, pp. 442–459, 2020.
- [37] H. R. Ahmadi and A. Vosoughi, "Impact of wireless channel uncertainty upon distributed detection systems," *IEEE Transactions on Wireless Communications*, vol. 12, no. 6, pp. 2566–2577, 2013.
- [38] A. Vosoughi and Y. Jia, "How does channel estimation error affect average sum-rate in two-way amplify-and-forward relay networks?" *IEEE Transactions on Wireless Communications*, vol. 11, no. 5, pp. 1676–1687, 2012.
- [39] Y. Jia and A. Vosoughi, "Transmission resource allocation for training based amplify-and-forward relay systems," *IEEE Transactions on Wireless Communications*, vol. 10, no. 2, pp. 450–455, 2011.
- [40] J. F. Shortle, J. M. Thompson, D. Gross, and C. M. Harris, *Fundamentals of queueing theory*. John Wiley & Sons, 2018, vol. 399.
- [41] R. Zhang, H. Chen, P. L. Yeoh, Y. Li, and B. Vucetic, "Full-duplex cooperative cognitive radio networks with wireless energy harvesting," in *2017 IEEE International Conference on Communications (ICC)*, 2017, pp. 1–6.
- [42] X. Guo, Y. He, S. Atapattu, S. Dey, and J. S. Evans, "Power allocation for distributed detection systems in wireless sensor networks with limited fusion center feedback," *IEEE Transactions on Communications*, vol. 66, no. 10, pp. 4753–4766, 2018.
- [43] H. Yazdani and A. Vosoughi, "On optimal sensing and capacity trade-off in cognitive radio systems with directional antennas," in *2018 IEEE Global Conference on Signal and Information Processing (GlobalSIP)*, Nov 2018, pp. 1015–1019.
- [44] S. M. Kay, *Fundamentals of statistical signal processing*. Prentice Hall PTR, 1993.
- [45] A. Vosoughi and A. Scaglione, "On the effect of receiver estimation error upon channel mutual information," *IEEE Transactions on Signal Processing*, vol. 54, no. 2, pp. 459–472, 2006.